Domains in Cell Plasma Membranes Investigated by Near-Field Scanning Optical Microscopy

Jeeseong Hwang,* Levi A. Gheber,* Leonid Margolis,# and Michael Edidin*
*Department of Biology, The Johns Hopkins University, Baltimore, Maryland 21218 USA, and #Moscow State University, Moscow, Russia

ABSTRACT Near-field scanning optical microscopy (NSOM) uses the near-field interaction of light from a sharp fiber-optic probe with a sample of interest to image surfaces at a resolution beyond the diffraction limit of conventional optics. We used NSOM to image fluorescently labeled plasma membranes of fixed human skin fibroblasts, either dried or in buffer. A patchy distribution of a fluorescent lipid analog suggestive of lipid domains was observed in the fixed, dried cells. The sizes of these patches were consistent with the sizes of domains implied by fluorescence photobleaching recovery measurements. Patches of fluorescent lipid analog were not spatially correlated with patches of transmembrane proteins, HLA class I molecules labeled with fluorescent antibody; the patchiness of the HLA class I molecules was on a smaller scale and was not localized to the same regions of membrane as the lipid analog. Sizes of HLA patches were deduced from a two-dimensional spatial autocorrelation analysis of NSOM images that resolved patches with radii of ~70 and ~600 nm on fixed, dried cells labeled with IgG and 300–600 nm on cells labeled with Fab and imaged in buffer. The large-size patches were also resolved by far-field microscopy. Both the spatial autocorrelation analysis and estimates from fluorescence intensity indicate that the small patches seen on fixed, dried cells contain ~25–125 HLA-I molecules each.

INTRODUCTION

Our view of cell membranes as two-dimensional (2D) fluids, all the constituents of which move freely (Singer and Nicolson, 1972), has been changed in recent years by demonstrations of lateral heterogeneities, patches, and domains in cell surface membranes (Edidin, 1996; Kusumi and Sako, 1996; Jacobson et al., 1995). Membrane domains have been defined mainly by measurements of the lateral diffusion of membrane proteins and lipids, although other methods have also been used (Saxton and Jacobson, 1997; Edidin, 1998). The measurements suggest that the size of many membrane domains is in the range of hundreds of nanometers, at or below the resolution of far-field microscopy.

Near-field scanning optical microscopy (NSOM) uses the contrast techniques of far-field microscopy but achieves resolution of surface structures well beyond the diffraction limit of far-field microscopy (Betzig and Trautman, 1992). We have used NSOM to image human fibroblasts labeled with both fluorescent phospholipid analogs and with fluorescent antibodies to membrane proteins, HLA class I (HLA-I) molecules. The patchiness of the fluorescence in our images of fixed, dehydrated cells is consistent with the size of membrane patches and domains inferred from other types of measurements performed on live cells; patches of HLA-I proteins are also seen in NSOM images of fixed cells scanned wet, in buffer. The larger patches observed by NSOM were also observable by conventional, far-field fluorescence microscopy of wet cells.

Received for publication 9 June 1997 and in final form 27 January 1998.

Address reprint requests to Dr. Michael Edidin, Department of Biology, The Johns Hopkins University, 34th and Charles Streets, Baltimore, MD 21218-2685. Tel.: 410-516-7294; Fax: 410-516-5213; E-mail: edidin@jhu.edu.

Dr. Hwang's current address: Optical Technology Division, National Institute of Standards and Technology, Gaithersburg, MD 20899.

Dr. Margolis's current address: Laboratory of Cellular and Molecular Biophysics, NICHD, National Institutes of Health, Bethesda, MD 20892.

0006-3495/98/05/2184/07 $2.00

MATERIALS AND METHODS

Cell culture

Normal human skin fibroblasts, strain 5659C, were obtained from the NIGMS Cell Repository, Coriell Institute (Camden, NJ) and were maintained in Dulbecco's modified Eagle's medium supplemented with 10% fetal calf serum (Intergen, Purchase, NY) and 2 mM L-glutamine at 37°C in a water-saturated atmosphere with 5% CO_2 in air. For microscopy, cells were plated onto glass coverslips (VWR Scientific, Baltimore, MD, 18-mm diameter number 1) for ~24 h in the same medium until the cell coverage reached ~50% of the surface of the coverslip. Properly cultured cells showed flat leading edges with several tens of square microns of microvillus-free plasma membrane. The relatively short time between plating the cells and observing ensured that the cultures contained little cell debris and that the cells themselves did not produce a large amount of extracellular matrix.

Cell labeling

All labeling was done at ~2°C to prevent the internalization or patching of the lipid analogs or membrane proteins. Cells cultured on a coverslip were washed three times with 1 ml of cold HEPES-buffered minimal essential medium (HMEM) and then either incubated for 20 min in 1 ml of HMEM with 5 μM 2-(4,4-difluoro-5,7-dimethyl-4-bora-3a,4a-diaza-s-indacene-3-pentanoyl)-1-hexadecanoyl-*sn*-glycero-3-phosphocholine (BODIPY-PC; D-3820 from Molecular Probes, Eugene, OR), complexed to defatted bovine serum albumin (BSA; Sigma Chemical Co., St. Louis, MO) (Chen et al., 1996; Pagano and Martin, 1988) or for 2 h in ~0.5 ml of HMEM containing ~0.3 mM tetramethylrhodamine-conjugated monoclonal immunoglobulin (IgG) to a monomorphic epitope of human major histocompatibility complex, HLA-I molecules, KE-2 (TMR-KE-2) (Schreiber et al., 1984). Preparation of IgGs and Fabs and conjugation procedures are described elsewhere (Edidin and Wei, 1982). For most experiments, the labeled cells were washed three times in cold HMEM, fixed for 10 min in

freshly prepared 3% formaldehyde and 0.05% glutaraldehyde, and then dried in a desiccator at 4°C. The sealed desiccator was warmed to room temperature before exposing the sample coverslip to the air. Cells for wet NSOM imaging were labeled with Fab KE-2 conjugated to the cyanine dye Cy3 (Mujumdar et al., 1993), fixed in 4% paraformaldehyde, and imaged in HEPES-buffered Hanks' balanced salt solution.

Cells labeled by the BODIPY-PC/BSA complex were brightly fluorescent in conventional far-field fluorescence microscopy (FFM). The labeling was apparently due to transfer of the BODIPY-PC from the BSA carrier to the cell surface membrane and not to adsorption of the BODIPY-PC/BSA complex. We infer this from the high mobile fraction of lipid analog (see Results) and from the fact that, in a control experiment, 5 μM BSA covalently coupled to the fluorophore Cy3 did not label cells observed by FFM.

FFM fluorescence images were obtained from cells imaged wet in the NSOM (see below). These images contain artifacts originating from the depth of their focal plane and limited lateral resolution. Thus, a larger fluorescence patch will appear brighter than a smaller one, even if the surface density of fluorophores is identical in both. There is an intrinsic correlation between the size and intensity of patches. For this reason, the larger patches contribute more to the autocorrelation function (because their intensity is higher) and the calculation exaggerates the size of the patches. To perform a size analysis based on the fluorescence image, we needed to remove the intensity information and retain only the size information. This was done by filtering a copy of the original image to obtain the low-frequency components that constitute the background. Then, the original image was divided by the background image, correcting in this way for the differences in intensity between clusters of different size.

Concanavalin A was covalently conjugated to preformed dipalmitoyl phosphatidylcholine (DPPC) liposomes, doped with glutaryl-dipalmitoyl phosphatidylethanolamine (DPPE) containing 0.1 mol % of the fluorescent lipid analog $DiIC_{18}$ (Molecular Probes). Liposomes were produced by sonicating the final lipid solution. For cell membrane staining the liposome stock solution, ~10 mM DPPC was diluted with HMEM to a final working concentration of ~500 μM DPPC.

Fluorescence photobleaching recovery measurements

Fluorescence photobleaching recovery (FPR) measurements were made on cells labeled as for NSOM but not fixed or dried. The spot-size-dependent FPR experiment is described in detail elsewhere (Yechiel and Edidin, 1987). In FPR, an attenuated laser beam is focused to a spot on a labeled cell surface, and the concentration of label is monitored in terms of fluorescence, $I_{(0)}$. A fraction of the fluorophores in the area are then bleached by brief (millisecond) exposure to the unattenuated laser beam. The beam is then again attenuated and is used to monitor the return of fluorescence to the bleached area as a function of time t, $I_{(t)}$. The diffusion coefficient D of the fluorescently labeled mobile molecules is calculated from the half-time for recovery and the area of the bleaching beam. $I_{(t)}$ almost always reaches an asymptote, $I_{max} < I_{(0)}$. $I_{max}/I_{(0)}$ yields R, the fraction of all labeled molecules mobile in the time and the length scales of the measurement.

Near-field scanning optical microscopy

The NSOM for imaging fixed, dried cells used an adiabatically tapered, Al-coated single-mode optical fiber probe with an aperture with a diameter that is typically ~80 nm. Blue (488-nm) light from a Kr/Ar laser or 543-nm light from a green He-Ne laser was coupled through the fiber probe for the excitation of BODIPY and rhodamine, respectively. The probe was scanned over the cell surface at a distance of <10 nm, resulting in spatial resolution of ~40 nm in fluorescence imaging. A corresponding shear force image, which shows the surface contour, was obtained simultaneously with each scan of fluorescence. Details of the NSOM are described elsewhere (Betzig et al., 1990). The NSOM used for wet cell imaging is similar to the one used for dry imaging in most respects, but it is built on an inverted, rather than an upright, far-field microscope and has a special sample holder and head that allows its operation in liquid (Gheber et al., 1998).

RESULTS AND DISCUSSION

We earlier used FPR to infer the existence of domains in human fibroblast plasma membranes (Yechiel and Edidin, 1987). We found that the apparent mobile fractions of labeled lipids and proteins decreased as the area bleached in a FPR measurement increased over the range 0.4–20 μm^2. This is not expected if molecules can diffuse freely over a membrane area of hundreds of square microns but is expected if diffusing molecules are confined in domains of a few square microns.

The labels used for our NSOM experiments of human fibroblast membranes, BODIPY-PC and TMR-KE2 monoclonal antibody (mAb; anti-HLA), showed the same behavior in FPR measurements as the labels in our earlier experiments. At 22°C, the average mobile fractions of a fluorescent lipid probe, BODIPY-PC, increased with decreasing size of the laser spot. Mobile fractions of 0.53 $\pm$ 0.07, 0.76 $\pm$ 0.10, and 0.86 $\pm$ 0.11 were obtained for the laser spots of 2.4, 1.4, and 0.8 μm ($1/e^2$ radius), respectively. Similarly, mobile fractions of HLA-I molecules labeled with TMR-KE-2 mAb were 0.53 $\pm$ 0.15, 0.62 $\pm$ 0.20, and 0.72 $\pm$ 0.13. Thus, using the criteria developed earlier (Yechiel and Edidin, 1987), it appears that the lipid analog BODIPY-PC and HLA-I proteins are concentrated in membrane domains.

Our NSOM proved equal to scanning the rugged surfaces of fixed, dried fibroblasts. Images of fibroblasts labeled with BODIPY-PC and TMR-KE2 mAb clearly displayed the patchy distributions of both labels. BODIPY-PC fluorescence was slightly concentrated over surface peaks, seen in the shear-force image. However, the greatest patchiness of fluorescence was found in smooth areas of the membrane. Fig. 1 *A* is typical of this distribution. It can be seen that in the topographically smooth area of membrane in the left of the figure the BODIPY-PC fluorescence is disrupted by fractal-like dark patches several hundred nanometers wide, indicating exclusion of the lipid analogs from some areas of the membrane. The length scale of the fluorescent regions surrounded by the dark patches is consistent with the length scale of lipid domains inferred from the FPR experiment described above. Although we do not understand the exact mechanism of the lipid exclusion, the fact that the shear-force image of the same area showed a continuous membrane made it evident that the dark patches were not artifacts of membrane damage (Fig. 1 *C*). Furthermore, the dark patches in the lipid analog image were bright in the TMR image in (Fig. 1 *B*); that is, HLA-I proteins were present, and possibly concentrated, in regions that excluded the lipid analog.

The fluorescence from labeled HLA-I proteins closely followed membrane contours, concentrating along ridges seen in the shear-force image (compare Fig. 1, *B* and *C*). In flat regions of membranes, fluorescence from labeled proteins did not have any large-scale pattern comparable to that seen for the lipid analog in Fig. 1 *A*. As noted above, the fluorescence was found in both lipid-rich and lipid-poor areas.

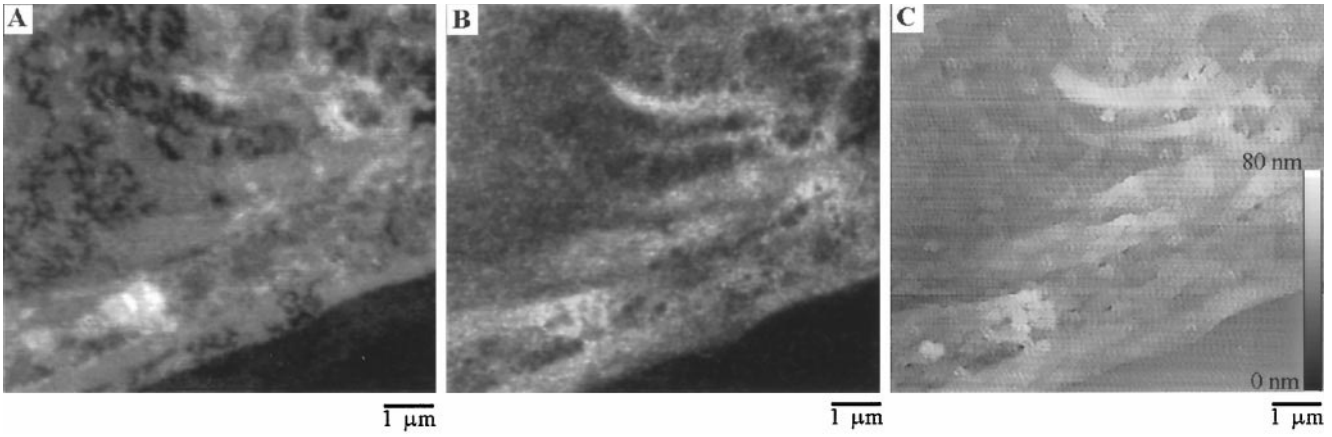

FIGURE 1 Images of human fibroblasts labeled with both the fluorescent lipid analog Bodipy-PC and a tetramethylrhodamine-conjugated monoclonal antibody, KE2, to the transmembrane protein HLA-I and then fixed and dried. (*A*) Near-field fluorescence image of the distribution of Bodipy-PC. The linear gray scale measures the fluorescence intensity from 1.0×10^2 cps/nW to 8.2×10^4 cps/nW. (*B*) Near-field fluorescence image of the distribution of class I MHC molecules labeled with TMR-KE2 monoclonal antibodies. Linear gray scale measures the fluorescence intensity from 1.0×10^2 cps/nW to 1.8×10^4 cps/nW. (*C*) Shear-force topographic image of the same cell. Inset gray scale displays the height of the surface topography.

The patchy distribution in the fluorescence image could result from the projection of the fluorescence signal distributed over protrusions from the cell surface. For a constant surface density of labeled molecules, there will be more fluorophores in the projection of a surface protrusion than in a flat region with the same surface area. This effect is seen as the commonly observed ring stain of fluorescently labeled cells observed by FFM. However, in near-field microscopy, the evanescent wave from the aperture, which excites fluorescence, decays exponentially away from the aperture. Therefore, only the fluorophores in this near-field range, typically within a few tens of nanometers, are effectively excited as the tip follows the surface topography at a constant height from the surface.

The fluorescence of BODIPY shifts from green to red at high concentrations of the lipid analog (cf. Chen et al., 1996). However, the patchiness in the BODIPY-PC image is not due to the wavelength dependence of the quantum efficiency of our detector. In fact, our silicon avalanche photon detector actually has a higher quantum efficiency at longer wavelengths. Even if this red fluorescence was blocked by the filter set used for acquiring the lipid fluorescence image, it would have appeared as a bright patch in the protein fluorescence image, but this is not the case. For example, note that the ragged dark regions at the edge of the cell (bottom of the image) in Fig. 1 *A* do not correspond to bright regions in the same part of the cell in Fig. 1 *B*.

We reasoned that, if HLA-I proteins were aggregated and/or confined to membrane domains, then a spatial autocorrelation analysis, analogous to the temporal autocorrelation fluorescence spectroscopy (Magde et al., 1978), would yield an autocorrelation function characterizing the spatial scale of intensity fluctuations. We calculate the normalized spatial 2D autocorrelation function of a digitized fluorescence NSOM image as

$$g(\underline{\xi}) = g(\xi_x, \xi_y) = [\langle i(\underline{\mathbf{r}})i(\underline{\mathbf{r}} + \underline{\xi})\rangle - \langle i(\underline{\mathbf{r}})\rangle]^2/\langle i(\underline{\mathbf{r}})\rangle^2, \quad (1)$$

where $\underline{\xi}$ is the spatial lag vector and $\langle\rangle$ is the average over the entire image. The averaged autocorrelation term in the numerator was obtained using a 2D fast Fourier transformation algorithm; the original image was Fourier transformed to obtain its 2D power spectrum matrix, and the matrix was then inversely Fourier transformed again (Press et al., 1992). The angle-averaged autocorrelation function, $g(\xi)$, the analog of the time-averaged autocorrelation function in the time domain, was obtained by averaging over all angles of the spatial lag vector $\underline{\xi}$, keeping the length of $\underline{\xi}$ fixed.

Time autocorrelation functions can be represented by two distinct time-dependent functions, one describing directed flow and one describing random diffusion (Magde, 1987). In the time domain, when individual fluorophores undergo

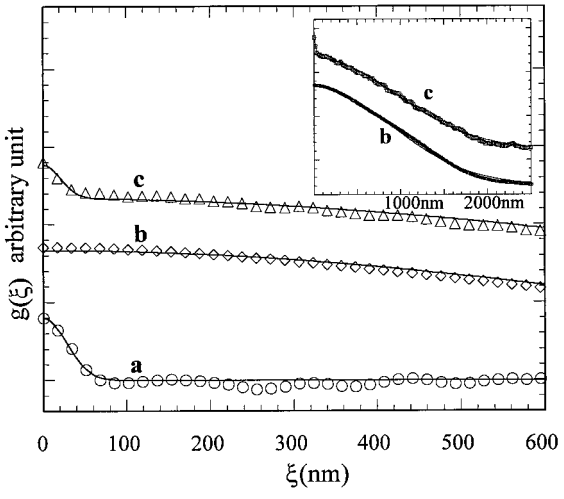

FIGURE 2 Angle-averaged 2D autocorrelation functions from simulated images containing clusters of different sizes: 35 nm (*a*) and 1000 nm (*b*). The same function is displayed in *c* for the image containing two different types of islands with different sizes: 20 nm and 1000 nm. The inset shows asymptotes of curves *b* and *c*.

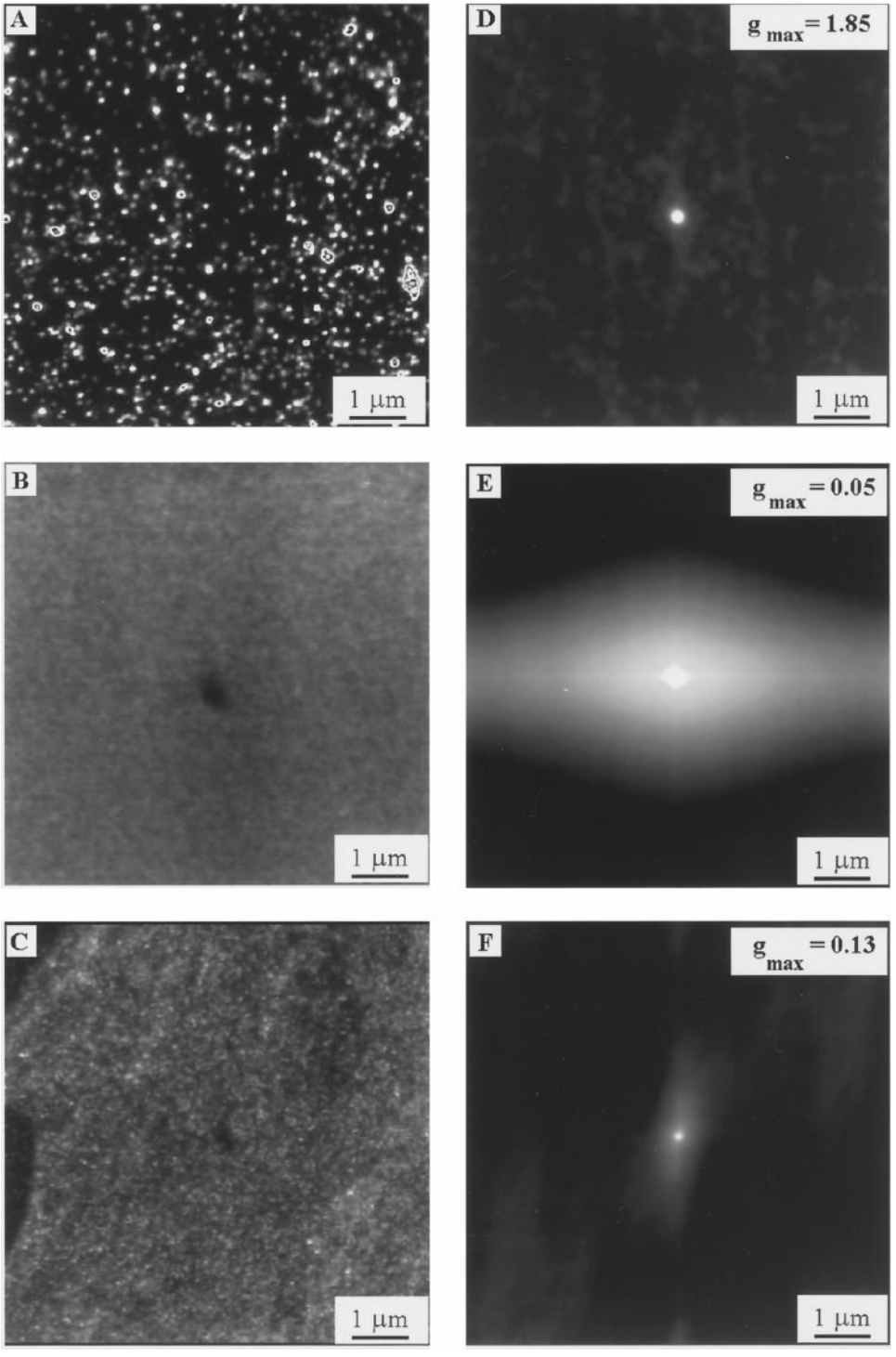

FIGURE 3 NSOM images and corresponding 2D autocorrelation images of a human skin fibroblast, fixed and dried after decorating with concanavalin-A-conjugated, $DiIC_{18}$-labeled DPPC liposomes (*A*), DPPC monolayer uniformly labeled with Bodipy-PE molecules (*B*), and a human skin fibroblast labeled with TMR-IgG against HLA membrane proteins. Corresponding 2D autocorrelation images, $g(\xi)$, are displayed in *D*, *E*, and *F*. g_{max} in each autocorrelation image represents $g(0,0)$ at the center.

uniform translation with an average velocity V across the measured sample volume enclosed by the area, πw^2, where w is the $1/e^2$ radius of the laser beam, the temporal autocorrelation function is

$$g(t) = g(0)\exp[-(t/t_f)^2], \quad (2)$$

where $t_f = w/V$ is the time interval for a fluorophore to move across the probing volume. This equation reflects consecutive detection events from a constituent fluorescent particle translating across the probing volume for a time interval t_f.

By analogy, patchiness of fluorescence, clustering of labeled molecules, can be determined from a spatial function equivalent to the directed flow function such as (Peterson et al., 1993)

$$g(\xi) = \sum_i g_i(0)\exp[-(\xi/\xi_i)^2], \quad (3)$$

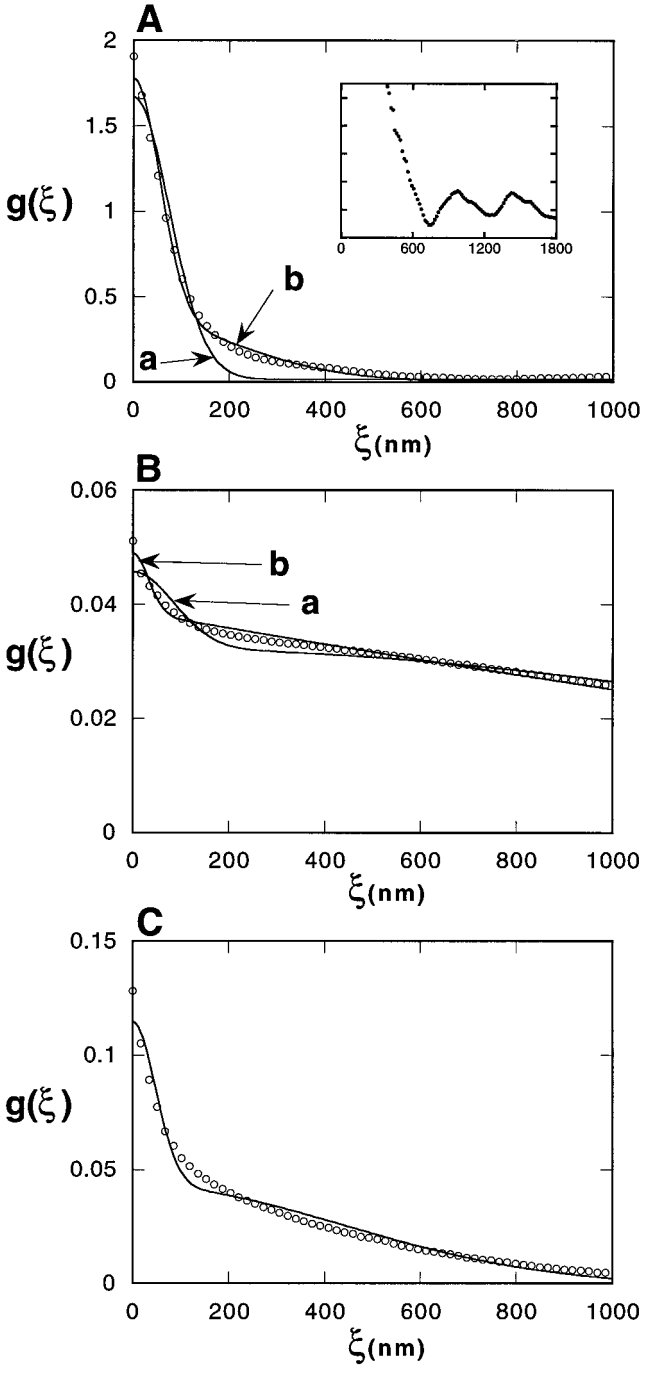

FIGURE 4 Angle-averaged autocorrelation plots for the images in Fig. 3. (*A*) A cell decorated with fluorescent DPPC liposomes. (*B*) Fluorescently labeled DPPC monolayer. (*C*) A cell labeled with TMR-IgG against HLA membrane proteins. In *A*, two curve fits are shown for a single Gaussian (*a*) and for two Gaussians (*b*). In *B*, two curve fits are with two Gaussians (*a*) and with the linear superposition of Gaussian involving clustered distribution of fluorophores and a non-Gaussian in Eq. 5, which reflects random distribution of them. In *C*, the fit with double Gaussians with the characteristic lengths of 67 and 623 nm is displayed.

where the total 2D autocorrelation is summed over distinct spatial frequency components, and ξ is the magnitude of the spatial lag vector for the autocorrelation calculation. The characteristic radii, ξ_i, are good measures of the average sizes of clusters, where index i represents each group of clusters with a given size.

When fluorescently labeled molecules randomly diffuse over the sample volume, the time autocorrelation may be written as

$$g(t) = g(0)[1 - t/t_d]^{-1}, \quad (4)$$

where $t_d = w^2/4D$, with D as the average diffusion constant of the fluorescently labeled molecules, which undergoes random diffusion. By analogy, when fluorophores are distributed in a random fashion, angle-averaged 2D spatial autocorrelation function may be fitted to

$$g(\xi) = g(0)[1 - \xi/\xi_i]^{-1}, \quad (5)$$

where ξ_d is a characteristic length of the random distribution of the fluorophores, which usually is larger than the size of the obtained image and is infinite for completely uniform distribution of fluorophores.

Before applying this spatial autocorrelation function to images of clustered molecules, we tested it against simulated images. Fig. 2 shows the angle-averaged spatial autocorrelation functions from three different images of clusters of known sizes. The points in Fig. 2 *a* show the autocorrelation function of islands with a Gaussian profile with a half-width at 1/e maximum (ξ) of 35 nm. Similarly, Fig. 2 *b* is the function for larger islands with a half-width at 1/e maximum (ξ) of 1000 nm. The least χ^2 fits with a single Gaussian function showed good agreement with the data points yielding a half-width at 1/e maximum of 39 and 1263 nm in each case. Next, the two images with two different sizes, 20 and 1000 nm, of islands were superimposed. From this image we calculated the autocorrelation and plotted the result in Fig. 2 *c*. The curve *c* clearly shows that the autocorrelation data fit well to the linear superposition of two Gaussians, so that the characteristic lengths of 29 and 1327 nm deduced from these fits are in good agreement with the sizes of islands in those images.

We next tested our spatial frequency analysis of clustering on NSOM images of cell membranes decorated with fluorescent liposomes, 100–300 nm in diameter, which do not fuse with the cell membrane (Fig. 3 *A*) and on images of a DPPC monolayer uniformly labeled with the fluorescent analog BODIPY-PE (Fig. 3 *B*). The NSOM image of the liposome-decorated membranes (Fig. 3 *A*) showed fluorescent islands of varying size and intensity; areas of membrane between the spots had the same low intensity as the coverslip, confirming that the fluorophore, $DiIC_{18}$, did not spread from liposomes to the cell membrane.

The spatial autocorrelation image of the liposome-decorated cells showed a pronounced peak at the origin, reflecting the existence of well defined spots (the liposomes) in the image (Fig. 3 *D*). In contrast, the spatial autocorrelation image of the monolayer had almost no intensity peak and a background near zero, the result expected for a noncorrelated, uniformly distributed fluorescence (Fig. 3 *E*). For the angle-averaged autocorrelation function, $g(\xi)$, the function

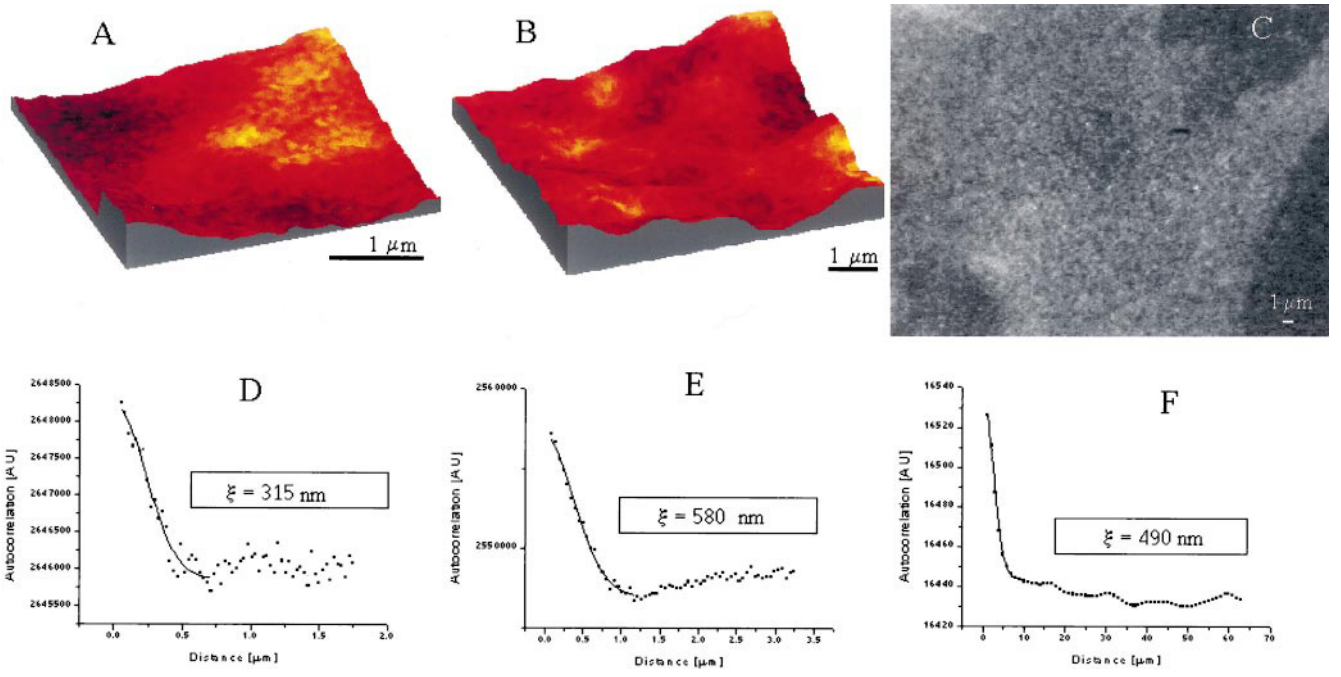

FIGURE 5 (*A* and *B*) Near-field images of a fixed human skin fibroblast acquired in liquid, labeled with Cy3-Fab KE-2 against HLA-I molecules. The 3D contours are from shear-force data and the color scale represents the fluorescence intensity. Topography height varies over a range of 165 nm (*A*) and 215 nm (*B*). (*C*) Far-field fluorescence image of the same cell. Autocorrelation profiles and Gaussian fits for the images in *A–C* yield characteristic lengths of 315 nm (*D*), 580 nm (*E*), and 490 nm (*F*).

for the liposome-decorated membrane was fit for small sizes by a single Gaussian, with $\xi = 110$ nm (Fig. 4 *A-a*). This characteristic length is slightly larger than expected by direct measurement of individual liposomes in the image. In fact, the curve was best fit for all scales by two Gaussians with $\xi_1 = 77$ nm and $\xi_2 = 309$ nm, resulting from the average radii of single liposomes as well as of aggregates of liposomes as seen in the NSOM image (Fig. 4 *A-b*). In addition, the distance between the first two peaks in the angle-averaged autocorrelation curve $g(\xi)$ measures ~450 nm as the average distance between neighboring liposomes (inset of Fig. 4 *A*) and reports ~310 liposomes in the image area, which is consistent with a visual count of the liposomes.

Spatial autocorrelation analysis of an image of uncorrelated, uniformly distributed fluorescence in a lipid monolayer was poorly fit by Gaussian functions as expected (Fig. 4 *B-a*). The best fit, in this case, was obtained by the linear superposition of a Gaussian on a small scale and a function equivalent to the time autocorrelation function for random diffusion on a larger scale (Fig. 4 *B-b*). The Gaussian peak at the origin with the 1/e decay length of 46 nm probably reflects the size of the aperture in the NSOM tip, although it may also reflect smaller-scale heterogeneity of fluorescence distribution.

Having tested our method of analysis on known images, we next used it to resolve clusters of labeled HLA-I proteins in fixed, dried fibroblast membranes (Fig. 3 *C*). The spatial autocorrelation image also showed a definite peak at the origin (Fig. 3 *F*). Although it is not a perfect fit, the spatial autocorrelation function of intensity was best fit by two Gaussians with $\xi_1 = 67$ nm and $\xi_2 = 623$ nm (Fig. 4 *C*). The smaller-size patch, ~70 nm radius, was also resolved when images were filtered to remove larger features (as described in Materials and Methods) and fitted to a single Gaussian. This size of these smaller patches is close to the radius of small clusters of HLA molecules in liposomes and cells estimated from rotational diffusion measurements (Chakrabarti et al., 1992; Damjanovich et al., 1995). The large, 623-nm radius or larger, clusters of HLA molecules approximate the size of membrane domains measured for many different proteins (Sheets et al., 1995) and are consistent with the FPR measurements showing restricted lateral diffusion of HLA molecules given above.

We were able to image fixed cells in buffer, using a modification of the original NSOM, built on an inverted far-field microscope, which allowed us to collect far-field and near-field images of the same cell, labeled with monovalent Fab fragments. Fig. 5 summarizes the results of these experiments. Fig. 5, *A* and *B*, shows near-field images of two different areas of the same cell. The images show both topography and fluorescence; the three-dimensional contours are drawn from the NSOM shear-force record, whereas the color scale represents the fluorescence intensity. Fig. 5, *D* and *E*, shows the autocorrelation profile for the fluorescence images in Fig. 5, *A* and *B*, respectively. The autocorrelation profiles of each image were fit by a single Gaussian with characteristic length of 315 nm (Fig. 5 *D*) and 580 nm (Fig. 5 *E*). Fig. 5 *C* shows a far-field image of the same cell imaged with the NSOM. The images in Fig. 5, *A* and *B*, were acquired approximately in the center of Fig. 5

C. The autocorrelation profile of the far field image in Fig. 5 *C* is shown in Fig. 5 *F*. Fitting it with a single Gaussian (after image filtering as described in Materials and Methods) yields a characteristic length of 490 nm.

It can be seen that the fluorescent patches in Fig. 5, *A* and *B*, vary considerably in size, even on the same cell, and even in areas close to one another. When imaging small areas (Fig. 5 *A*, for instance, is a 3.5 × 3.5 μm^2 scan), it is possible to distinguish different characteristic patch sizes. When imaging large areas, the patch radius obtained from autocorrelation analysis reflects an average size. It is not surprising, therefore, that the dimension calculated from the far-field image is somewhere between the dimensions observed by NSOM.

We also used NSOM to estimate the average number of proteins within the area of small patches on fixed and dried cells. As the optical cross section of a molecule is much larger than the physical size, to the first approximation, the fluorescence intensity is the summation of emissions from each fluorophore in a single patch. The typical local maximum of photon emission intensity measured from the image was ~12,200 counts per second per nanowatt of the tip pump power, corresponding to an average of ~20 fluorophores per patch (Hwang et al., 1995). The fluorophore to antibody ratio of our preparation was ~0.8, and the quantum yield of TMR ranges between 0.2 and ~1, depending upon its environment. Hence each patch represents between 25 and 125 antibody molecules and at least that number of HLA-I molecules. These values are consistent with those measured for purified HLA-I molecules forming patches in liposomes (Chakrabarti et al., 1992)

CONCLUSIONS

Our high-resolution fluorescence NSOM images of the distributions of lipids and proteins in plasma membranes of fixed and dried human skin fibroblasts are consistent with other data indicative of patches and membrane domains on a scale of tens to hundreds of nanometers, including recent observations of cells by atomic force microscopy (Jenei et al., 1997). Both NSOM and far-field results on wet cells are in excellent agreement with the results obtained on dried cells for the large-scale clusters. NSOM of wet cell images, however, fail to reveal the small-scale features (67 nm) observed on dried cells. We believe this to be due to the early stages of development and relatively difficult operation of the instrument in liquid on wet and soft cells. Dehydrating the cells appears not to introduce artifacts in the NSOM images of labeled HLA proteins, at least at the scale of hundreds of nanometers.

We thank Dr. Eric Betzig for his technical guidance in NSOM and Dr. Larissa Gordeeva for help with the liposome preparation.

This work was supported by National Institutes of Health grants P01 DK44375, R37 AI14584, and R03 TW00086 (FIRCA) to M. Edidin.

REFERENCES

Betzig, E., P. L. Finn, and J. S. Weiner. 1990. Combined shear force and near-field scanning optical microscopy. *Appl. Phys. Lett*. 60:2484–2486.

Betzig, E., and J. K. Trautman. 1992. Near-field optics: microscopy, spectroscopy, and surface modification beyond the diffraction limit. *Science*. 257:189–195.

Chakrabarti, A., J. Matko, N. A. Rahman, B. G. Barisas, and M. Edidin. 1992. Self-association of class I major histocompatibility complex molecules in liposome and cell surface membranes. *Biochemistry*. 31: 7182–7189.

Chen, C-S., O. C. Martin, and R. E. Pagano. 1996. Changes in the spectral properties of a plasma membrane lipid analog during the first seconds of endocytosis in living cells. *Biophys. J.* 72:37–50.

Damjanovich, S., G. Vereb, A. Schaper, A. Jenei, J. Matko, J. P. P. Starink, G. Q. Fox, D. J. Arndt-Jovin, and T. M. Jovin. 1995. Structural hierarchy in the clustering of HLA class I molecules in the plasma membrane of human lymphoblastoid cells. *Proc. Natl. Acad. Sci. U.S.A*. 92: 1122–1126.

Edidin, M. 1996. Getting there is only half the fun. *Curr. Top. Membr.* 43:1–13.

Edidin, M. 1998. Lipid microdomains in cell surface membranes: transience and stability in the lateral organization of phospholipid bilayers. *Curr. Opin. Struct. Biol.* 7:528–532.

Edidin, M., and T. Wei. 1982. Lateral diffusion of H-2 antigens on mouse fibroblasts. *J. Cell Biol*. 95:458–462.

Gheber, L. A., J. Hwang, and M. Edidin. 1998. Design and optimization of a near-field scanning optical microscope for imaging biological samples in liquid. *Appl. Opt.* 7:528–532.

Hwang, J., L. K. Tamm, C. Bohm, T. S. Ramalingam, E. Betzig, and M. Edidin. 1995. Nanoscale complexity of phospholipid monolayers investigated by near-field scanning optical microscopy. *Science*. 270: 610–614.

Jacobson, K., E. D. Sheets, and R. Simson. 1995. Revisiting the fluid mosaic model of membranes. *Science*. 268:1441–1442.

Jenei, A., S. Varga, L. Bene, L. Matyus, A. Bodnar, Z. Bacso, C. Pieri, R. Gaspar, Jr., T. Farkas, and S. Damjanovich. 1997. HLA class I and II antigens are partially co-clustered in the plasma membrane of lymphoblastoid cells. *Proc. Natl. Acad. Sci. U.S.A*. 94:7269–7274.

Kusumi, A., and Y. Sako. 1996. Cell surface organization by the membrane skeleton. *Curr. Opin. Cell Biol*. 8:566–574.

Magde, D., W. Webb, and E. L. Elson. 1978. Fluorescence correlation spectroscopy. III. Uniform translation and laminar flow. *Biopolymers*. 17:361–376.

Mujumdar, R. D., L. A. Ernst, S. R. Mujumdar, C. J. Lewis, and A. S. Waggoner. 1993. Cyanine dye labeling reagents: sulfoindocyanine succimidyl esters. *Bioconjugate Chem.* 4:105–111.

Pagano, R. E., and O. C. Martin. 1988. A series of fluorescent *N*-acylsphingosides: synthesis, physical properties and studies in cultured cells. *Biochemistry*. 27:4439–4445.

Peterson, N. O., P. L. Hoddelius, P. W. Weisman, O. Seger, and K. Magnusson. 1993. Quantitation of membrane receptor distributions by image correlation spectroscopy: concept and application. *Biophys. J.* 65:1135–1146.

Press, W. H., S. A. Teukolsky, W. T. Vetterling, and B. P. Flannery. 1992. Numerical Recipes in C, 2nd ed. Cambridge Press, New York. 496–532.

Saxton, M. J., and K. Jacobson. 1997. Single-particle tracking: applications to membrane dynamics. *Annu. Rev. Biophys. Biomol. Struct.* 26: 373–399.

Schreiber, A. B., J. Schlessinger, and M. Edidin. 1984. Interaction between major histocompatibility complex antigens and epidermal growth factor receptors on human cells. *J. Cell Biol*. 98:725–731.

Sheets, E. D., R. Simson, and K. Jacobson. 1995. New insights into membrane dynamics from the analysis of cell surface interactions by physical methods. *Curr. Opin. Cell Biol*. 7:707–714.

Singer, S. J., and G. L. Nicolson. 1972. The fluid mosaic model of the structure of cell membranes. *Science*. 175:720–731.

Yechiel, E., and M. Edidin. 1987. Micrometer-scale domains in fibroblast plasma membranes. *J. Cell. Biol*. 105:755–760.